

Targeting hepatic glutaminase activity to ameliorate hyperglycemia

Russell A Miller^{1,2,13}, Yuji Shi^{2,13}, Wenyun Lu^{3,13}, David A Pirman⁴, Aditi Jatkar², Matthew Blatnik⁴, Hong Wu⁴, César Cárdenas^{5–8}, Min Wan², J Kevin Foskett^{9,10} , Junyoung O Park^{3,11} , Yiyi Zhang¹², William L Holland¹² , Joshua D Rabinowitz³ & Morris J Birnbaum^{1,2,10} 

Glucagon levels increase under homeostatic, fasting conditions, promoting the release of glucose from the liver by accelerating the breakdown of glycogen (also known as glycogenolysis). Glucagon also enhances gluconeogenic flux, including from an increase in the hepatic consumption of amino acids¹. In type 2 diabetes, dysregulated glucagon signaling contributes to the elevated hepatic glucose output and fasting hyperglycemia that occur in this condition. Yet, the mechanism by which glucagon stimulates gluconeogenesis remains incompletely understood. Contrary to the prevailing belief that glucagon acts primarily on cytoplasmic and nuclear targets, we find glucagon-dependent stimulation of mitochondrial anaplerotic flux from glutamine that increases the contribution of this amino acid to the carbons of glucose generated during gluconeogenesis. This enhanced glucose production is dependent on protein kinase A (PKA) and is associated with glucagon-stimulated calcium release from the endoplasmic reticulum, activation of mitochondrial α -ketoglutarate dehydrogenase, and increased glutaminolysis. Mice with reduced levels of hepatic glutaminase 2 (GLS2), the enzyme that catalyzes the first step in glutamine metabolism, show lower glucagon-stimulated glutamine-to-glucose flux *in vivo*, and GLS2 knockout results in higher fasting plasma glucagon and glutamine levels with lower fasting blood glucose levels in insulin-resistant conditions. As found in genome-wide association studies (GWAS), human genetic variation in the region of *GLS2* is associated with higher fasting plasma glucose^{2,3}; here we show in human cryopreserved primary hepatocytes *in vitro* that these natural gain-of-function missense mutations in *GLS2* result in higher glutaminolysis and glucose production. These data emphasize the importance of gluconeogenesis from glutamine, particularly in pathological

states of increased glucagon signaling, while suggesting a possible new therapeutic avenue to treat hyperglycemia.

Nearly 50 years ago, it was observed that glucagon-dependent increases in glucose production in perfused rat liver were associated with immediate changes in protein phosphorylation resulting from enhanced cyclic AMP (cAMP) production⁴. Subsequent work identified PKA-mediated phosphorylation events that work in concert to increase gluconeogenesis and glycogenolysis in response to glucagon¹. While these actions of glucagon are the key drivers of acute stimulation of hepatic glucose production, during longer fasting, the glucagon-stimulated uptake and oxidation of amino acids—in concert with their release from skeletal muscle—provides access to an additional pool of gluconeogenic substrates to further support fasting glucose production and the proper maintenance of systemic glucose levels.

Whereas lactate provides the largest and most well-studied source of carbon for gluconeogenesis, amino acids also contribute to gluconeogenesis, with glutamine potentially being important given its role as a physiological nitrogen shuttle⁵. We therefore set out to test the impact of glucagon on the metabolic flux of lactate and glutamine in mouse primary hepatocytes. Hepatocytes isolated from fasted mice were incubated with physiologically relevant ratios of lactate and glutamine with only one of the substrates labeled with ¹³C [U-¹³C]lactate:[¹²C]glutamine or [¹²C]lactate:[U-¹³C]glutamine. In each of these conditions, glucagon was equally capable of stimulating an increase in glucose production from the labeled cells after 60 min of treatment (Fig. 1a,b). The isotopic distribution of extracellular glucose was analyzed under these conditions and showed a marked change with glucagon treatment (Fig. 1a–d). Glucagon treatment resulted in a reduction in the fractional contribution of lactate to glucose and an increase in the input of glutamine (Fig. 1c,d). Intracellular metabolites were also assessed over time in the same experiments to map the

¹Institute for Diabetes, Obesity, and Metabolism, Perelman School of Medicine, University of Pennsylvania, Philadelphia, Pennsylvania, USA. ²Pfizer Internal Medicine Research Units, Cambridge, Massachusetts, USA. ³Chemistry and Integrative Genomics, Princeton University, Princeton, New Jersey, USA. ⁴Pfizer Worldwide Research and Development, Groton, Connecticut, USA. ⁵Anatomy and Developmental Biology Program, Institute of Biomedical Sciences, University of Chile, Santiago, Chile. ⁶Geroscience Center for Brain Health and Metabolism, Santiago, Chile. ⁷Buck Institute for Research on Aging, Novato, California, USA. ⁸Department of Chemistry and Biochemistry, University of California, Santa Barbara, Santa Barbara, California, USA. ⁹Department of Physiology, Perelman School of Medicine, University of Pennsylvania, Philadelphia, Pennsylvania, USA. ¹⁰Department of Cell and Developmental Biology, Perelman School of Medicine, University of Pennsylvania, Philadelphia, Pennsylvania, USA. ¹¹Department of Chemical and Biological Engineering, Princeton University, Princeton, New Jersey, USA. ¹²Touchstone Diabetes Center, Department of Internal Medicine, University of Texas Southwestern Medical Center, Dallas, Texas, USA. ¹³These authors contributed equally to this work. Correspondence should be addressed to M.J.B. (morris.birnbaum@pfizer.com) or R.A.M. (russell.miller@pfizer.com).

Received 12 May 2014; accepted 8 February 2018; published online 26 March 2018; corrected online 12 June 2018; doi:10.1038/nm.4514

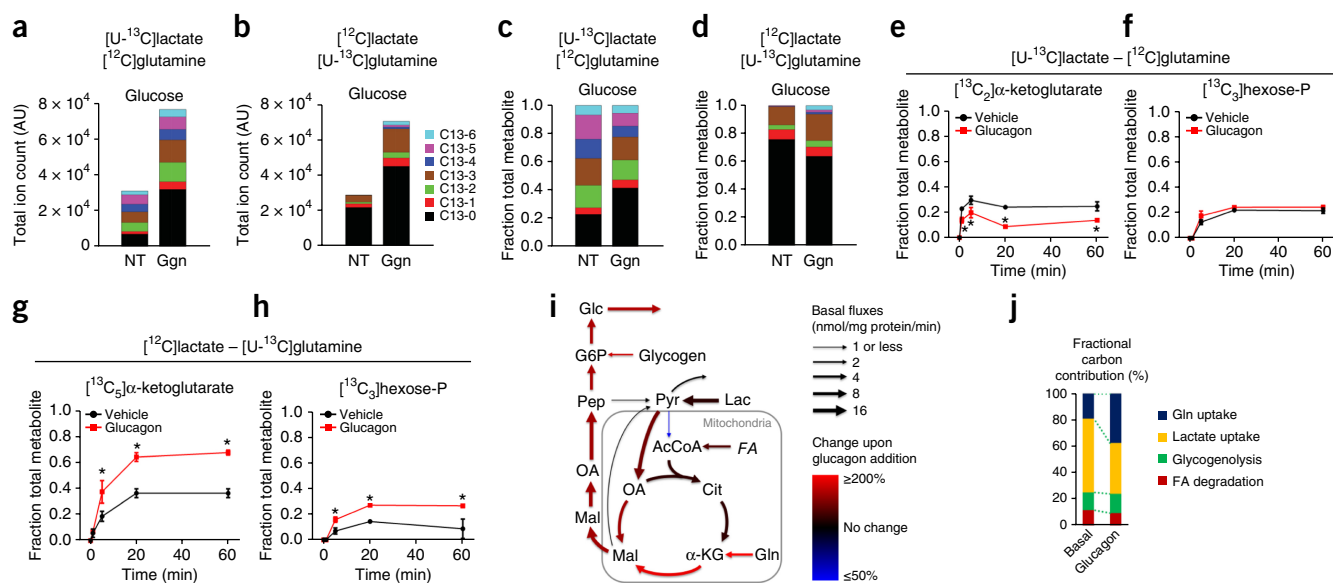


Figure 1 Glucagon-mediated metabolic flux studies from glutamine in primary hepatocytes. (**a–d**) Absolute amounts of extracellular glucose isotopomers (**a,b**) and relative amounts of extracellular glucose isotopomers (**c,d**) in primary hepatocytes isolated from fasted mice after plating for 4 h on collagen-coated plates and incubation with 5 mM [U-¹³C]lactate and 2.5 mM [¹²C]glutamine or 5 mM [¹²C]lactate and 2.5 mM [U-¹³C]glutamine. Cells were treated with glucagon (Ggn) or PBS vehicle (NT). Specific isotopomers of glucose are colored according to the number of ¹³C carbons. (**e–h**) Mass spectrometry analysis of intracellular metabolites from primary hepatocytes treated with PBS vehicle or glucagon and incubated with 5 mM [U-¹³C]lactate and 2.5 mM [¹²C]glutamine (**e,f**) or 5 mM [¹²C]lactate and 2.5 mM [U-¹³C]glutamine (**g,h**). For each metabolite, the most abundant isotopomer derived from the ¹³C-labeled substrate is displayed. Each time point represents the mean and standard error of three replicate samples. This experiment was repeated more than three times. (**i**) Graphical representation of fluxes determined by metabolic flux analysis of the data presented in **Figure 1** and **Supplementary Figures 1** and **2**. Net fluxes for the indicated reaction are expressed as nmol/mg protein per minute. (**j**) Fractional contribution of carbon as determined from modeling of the data presented in this figure and **Supplementary Figures 1** and **2**. FA, fatty acids; AcCoA, acetyl-CoA; Cit, citrate; α-KG, α-ketoglutarate; Gln, glutamine; Mal, malate; OA, oxaloacetate; Pep, phosphoenolpyruvate; Pyr, pyruvate; G6P, glucose-6-phosphate; Glc, glucose.

metabolic flux underlying the switch in gluconeogenic substrates. In the presence of [U-¹³C]lactate and [¹²C]glutamine, key tricarboxylic acid (TCA) metabolites showed a modest glucagon-stimulated decrease in labeling (**Fig. 1e,f** and **Supplementary Fig. 1**). In contrast, cells incubated in [¹²C]lactate and [U-¹³C]glutamine showed a large increase in the contribution of glutamine carbon to intracellular metabolites following glucagon treatment (**Fig. 1g,h** and **Supplementary Fig. 2**). After glucagon stimulation, there was robust generation of [¹³C₅]α-ketoglutarate, leading to an approximately 40% enrichment at steady state (**Fig. 1g** and **Supplementary Fig. 2**).

To obtain a quantitative view of underlying metabolic changes, we modeled the metabolic flux distribution that was consistent with the observed ¹³C labeling data (**Fig. 1i,j**, **Supplementary Fig. 3**, and **Supplementary Table 1**). Glucagon stimulated pyruvate carboxylase flux about 1.5-fold, while glutaminolysis was increased about 3-fold, resulting in a shift from lactate to glutamine as the gluconeogenic substrate. In summary, these results demonstrate that, although lactate is the greater source of gluconeogenic substrate under basal and hormone-stimulated conditions, the contribution of glutamine carbons to newly synthesized glucose is more greatly enriched in response to glucagon stimulation.

When primary hepatocytes were provided with lactate as the sole gluconeogenic substrate, glucagon elicited a reduction of α-ketoglutarate levels within 1 min that persisted for the duration of the 1-h experiment (**Fig. 2a**). Intracellular glutamate levels also fell in response to glucagon (**Fig. 2b**). In contrast, glucagon only transiently reduced α-ketoglutarate levels in the presence of [¹²C]lactate and [U-¹³C]glutamine, presumably owing to the contribution of glutamine

to anaplerosis (**Fig. 2c**). The recovery of α-ketoglutarate levels was accompanied by an increased fraction of [¹³C₅]α-ketoglutarate, indicating increased formation of α-ketoglutarate from glutamine (**Fig. 2d**). In the presence of glutamine, glucagon no longer caused a reduction of intracellular glutamate but instead increased the levels after 10 min (**Fig. 2e,f**). Glucagon treatment did not result in changes in the levels of intracellular glutamine (**Supplementary Fig. 4**).

The glucagon-dependent decrease in α-ketoglutarate in primary hepatocytes was confirmed using a biochemical assay; moreover, glucagon administered *in vivo* elicited a reduction in hepatic α-ketoglutarate (**Supplementary Fig. 5a,b**). Consistent with the increased α-ketoglutarate flux, mitochondria isolated from glucagon-treated cells displayed activation of α-ketoglutarate dehydrogenase (AKGDH) (**Supplementary Fig. 5c**). These data suggest that an immediate effect of glucagon in the liver is the stimulation of gluconeogenesis from glutamine, at least in part through activation of AKGDH. In addition to glucagon, dibutyryl-cAMP effectively reduced α-ketoglutarate levels in primary hepatocytes, indicating that, like the effects of glucagon, stimulation of AKGDH was mediated by activation of adenylate cyclase and increases in intracellular cAMP (**Supplementary Fig. 5a**).

To test whether PKA was required for the effects of glucagon, mice were infected with a recombinant adeno-associated virus vector that contained a hepatocyte-specific promoter controlling the expression of a mutant PKA regulatory subunit (PKA-RIα) that is unable to bind cAMP and thus behaves like a dominant inhibitor (AAV-PKA-DN)^{6,7}. While glucagon was able to increase glucose output and lower α-ketoglutarate levels in control cells, it failed to

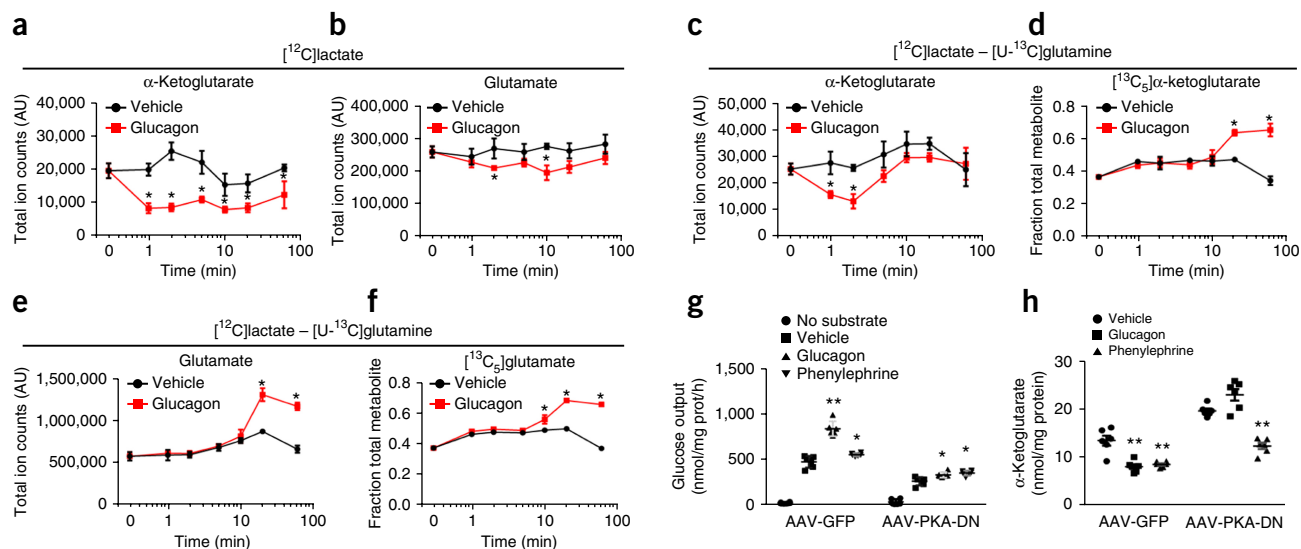


Figure 2 Kinetics effects of glucagon on α -ketoglutarate and glutamate in primary hepatocytes. (a–d) α -Ketoglutarate and glutamate levels when only $[^{12}\text{C}]$ lactate was provided as substrate (a,b) or when both $[^{12}\text{C}]$ lactate and $[^{13}\text{C}]$ glutamine were provided as substrates (c,d). (e,f) $[^{12}\text{C}]$ α -Ketoglutarate and $[^{13}\text{C}]$ glutamate fractions of total metabolites when both $[^{12}\text{C}]$ lactate and $[^{13}\text{C}]$ glutamine were present as extracellular substrates. Values represent triplicates from a pool of hepatocytes from four mice and are shown as the mean \pm s.e.m. This experiment was performed once, but the effect on α -ketoglutarate was examined in experiments repeated more than five times. (g,h) Glucose production (g) and enzymatic measurement of α -ketoglutarate (h) in primary hepatocytes from mice previously infected with AAV-TBG-GFP or AAV-TBG-PKA-DN. * $P < 0.05$, ** $P < 0.01$, two-tailed Student's *t*-test.

stimulate glucose output and reduce cellular α -ketoglutarate levels in cells infected with AAV-PKA-DN (Fig. 2g,h). In these same cells, glucagon-dependent phosphorylation of the PKA target proteins PFK1, inositol 1,4,5-trisphosphate receptor (IP₃R), and CREB was significantly attenuated by AAV-PKA-DN (Supplementary Fig. 5d). Pharmacological inhibition of PKA with H89 also blocked the changes in glucose output and α -ketoglutarate levels in response to glucagon (Supplementary Fig. 5e,f). These data show that, like the cytoplasmic and nuclear actions of glucagon, hormone-dependent alterations in mitochondrial metabolism require activation of PKA.

We investigated Ca^{2+} as a potential mediator of the actions of glucagon on TCA cycle flux. In primary mouse hepatocytes, glucagon elicited an increase in the concentration of intracellular Ca^{2+} derived from intracellular stores (Supplementary Fig. 5g). PKA phosphorylates IP₃R, an endoplasmic reticulum (ER) Ca^{2+} -release channel, enhancing its sensitivity to IP₃ (ref. 8). IP₃R phosphorylation was absent in cells infected with AAV-PKA-DN, indicating its dependence on the cAMP–PKA signaling pathway (Supplementary Fig. 5d).

The α -1 adrenergic receptor agonist phenylephrine activates phospholipase-C and causes an IP₃-dependent increase in intracellular Ca^{2+} concentration⁸. Unlike glucagon, phenylephrine did not stimulate phosphorylation of the PKA substrates PFK1, CREB, or IP₃R (Supplementary Fig. 5d). Phenylephrine treatment resulted in only a modest impact on glucose output but equivalent reductions in α -ketoglutarate levels as compared to glucagon; infection with AAV-PKA-DN had no impact on the effects of phenylephrine (Fig. 2g,h). In primary hepatocytes incubated with $[^{13}\text{C}]$ glutamine and $[^{12}\text{C}]$ lactate, glucagon and phenylephrine similarly enhanced the fractional labeling of extracellular glucose and intracellular metabolites (Supplementary Fig. 5h–i). In contrast, glucagon more strongly stimulated glucose synthesis and the total amount of ^{13}C incorporation from glutamine into glucose (Supplementary Fig. 5h). These data provide evidence that both glucagon and phenylephrine use Ca^{2+}

as an intracellular signal to enhance AKGDH activity, thereby biasing substrate selection for gluconeogenesis toward glutamine.

We next tested whether engineered reduction in hepatic glutaminase by knockdown of hepatic *Gls2* gene expression was sufficient to alter systemic glucose homeostasis in mice *in vivo*. Infection of mice with AAV2/8 virus that expressed an shRNA targeting the *Gls2* gene (AAV-GLS2-sh) lowered GLS2 protein levels (Fig. 3a). We performed *in vivo* infusion studies with $[^{13}\text{C}]$ glutamine and either saline or glucagon, and then monitored hepatic metabolites by mass spectrometry. As was observed in primary hepatocytes, in the mice infected with the negative-control AAV-GFP, glucagon caused a ~3-fold increase in the contribution of glutamine to glucose that was absent in mice infected with the AAV-GLS2-sh virus (Fig. 3b). Glucagon also caused a glutaminase-dependent increase in the fractional labeling of glycerol-3-phosphate in control liver, although the numerical increase failed to achieve statistical significance (Fig. 3c). The TCA cycle metabolites glutamate and malate exhibited reduced labeling at baseline in AAV-GLS2-sh-treated mice, indicating reduced glutamine-to-glutamate flux, but their labeling in control and glutaminase-knockdown liver was unaffected by glucagon (Supplementary Fig. 6a,b). This unexpected finding might be the result of the restricted periportal expression of GLS2 and glutamine-derived gluconeogenesis⁹.

We next examined the role of GLS2 knockdown on systemic glucose homeostasis. Despite a reduction in the contribution of glutamine to hepatic glucose in AAV-GLS2-sh-injected animals, there was no significant lowering of blood glucose as compared to control animals (Fig. 3d). However, the concentration of insulin was significantly reduced in plasma from AAV-GLS2-sh-injected mice, indicating enhanced insulin sensitivity (Fig. 3e). Consistent with this notion, intracellular markers of insulin action, IR β and AKT phosphorylation, were also lower in the livers of AAV-GLS2-sh-infected mice (Fig. 3a). These data indicate that, despite the lack of change in glucose levels

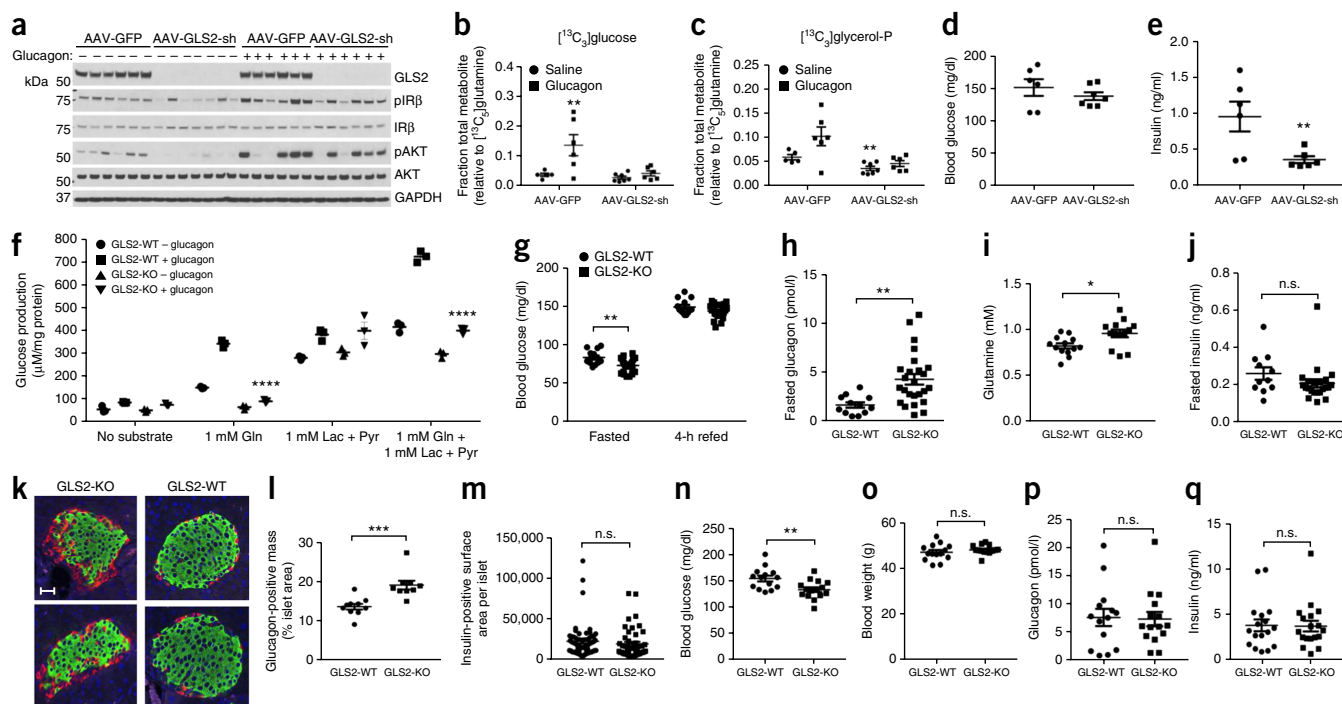


Figure 3 *In vivo* glutamine and glucagon infusion study from mice infected with AAV-GFP or AAV-GLS2-sh. **(a)** Western blot from liver tissue of GLS2, phosphorylated and total insulin receptor β (IR β), phosphorylated and total AKT, and GAPDH. **(b,c)** Hepatic [$^{13}\text{C}_3$]glucose **(b)** and [$^{13}\text{C}_3$]glycerol **(c)** normalized to the tissue [$^{13}\text{C}_3$]glutamine fraction. **(d,e)** Blood glucose **(d)** and plasma insulin **(e)** measured following infusion. In all panels, values represent the mean of at least five biological replicates. These experiments were performed once. **(f)** Glucose production from primary hepatocytes obtained from fasted GLS2-WT or GLS2-KO mice with the indicated substrates: 1 mM glutamine and/or 1 mM lactate + 0.1 mM pyruvate in the presence or absence of 100 nM glucagon for 1 h. Values represent the results from three biological replicates. **(g–m)** GLS2-WT and GLS2-KO mice were fed a chow diet. Animals were evaluated for fed and fasted blood glucose **(g)**, fasted plasma glucagon **(h)**, fasted plasma glutamine **(i)**, and fasted plasma insulin **(j)**. WT:KO = 13:25. **(k)** Representative immunofluorescence of glucagon (red) and insulin (green) in pancreatic islets of mice fasted overnight, merged with DAPI (blue). Scale bar, 30 μm . **(l)** Quantification of glucagon-positive mass per islets from mice fasted overnight. WT:KO = 10:9. **(m)** Quantification of insulin-positive surface area per islets from mice fasted overnight. **(n–q)** GLS2-WT and GLS2-KO mice were fed a high-fat diet for 17 weeks. Animals were evaluated for fasted blood glucose **(n)**, body weight **(o)**, fasted plasma glucagon **(p)**, and fasted plasma insulin **(q)**. Throughout, data are shown as means \pm s.e.m. * $P < 0.05$, two-tailed Student's *t*-test; n.s., not significant.

following knockdown of GLS2, the lesser requirement of insulin to maintain normoglycemia indicated enhanced insulin sensitivity.

To better understand the contribution of GLS2 to glucose homeostasis, we generated germline GLS2 knockout (KO) mice; the absence of GLS2 protein in hepatocytes was confirmed by western blot (**Supplementary Fig. 6c**). Primary hepatocytes were isolated from fasted GLS2 wild-type (WT) or GLS2-KO mice and subjected to glucose output assays (**Fig. 3f**). With physiological levels of glutamine as the sole substrate at 1 mM, glucagon stimulated glucose production in GLS2-WT but not GLS2-KO hepatocytes. In contrast, glucose production from lactate was similar in GLS2-WT and GLS2-KO primary hepatocytes. When both lactate and glutamine were provided as substrates, GLS2-KO primary hepatocytes produced less glucose at baseline and were less responsive to glucagon. These data indicate that GLS2 is an essential enzyme for glucagon-induced flux from glutamine to glucose in primary hepatocytes.

We next examined whether systemic glucose homeostasis was altered by loss of GLS2. GLS2-KO mice showed a reduction in blood glucose levels after overnight fasting but no change 4 h after refeeding (**Fig. 3g**). Fasting plasma glucagon (**Fig. 3h**) and glutamine (**Fig. 3i**) levels were significantly higher in GLS2-KO mice, with no change in insulin levels (**Fig. 3j**), indicating glucagon resistance in the liver. To investigate the underlying mechanism responsible for the elevation

of glucagon in GLS2-KO mice, we measured alpha and beta cell mass in pancreatic islets from fasted mice (**Fig. 3k**). Pancreatic islets from GLS2-KO mice demonstrated alpha cell hyperplasia (**Fig. 3l**), with no significant changes in beta cell mass (**Fig. 3m**).

To understand the importance of GLS2 in a disease setting, mice were challenged with a 60% high-fat diet. After 17 weeks on this diet, GLS2-KO mice exhibited a significant reduction in fasting glucose levels without significant changes in body weight, insulin, or glucagon (**Fig. 3n–q**). Taken together, these data support an important function of GLS2 in mediating the glucose output in fasting in response to glucagon.

Common genetic variants in a locus that includes the human liver glutaminase gene (*GLS2*) are associated with body mass index (BMI)-adjusted fasting plasma glucose and plasma glutamine levels^{2,3}. A common variation resulting in replacement of Leu581 by proline (p.Leu581Pro) is the polymorphism most highly associated with higher fasting plasma glucose and lower plasma glutamine. To determine whether this association is the result of higher glutaminase flux, we genotyped cryopreserved human hepatocytes and identified six lots heterozygous for the allele with the p.Leu581Pro substitution (L581/P581) and six lots homozygous for the major allele encoding Leu581 (L581/L581) that were matched for available donor characteristics. Hepatocytes from L581/P581 donors exhibited greater

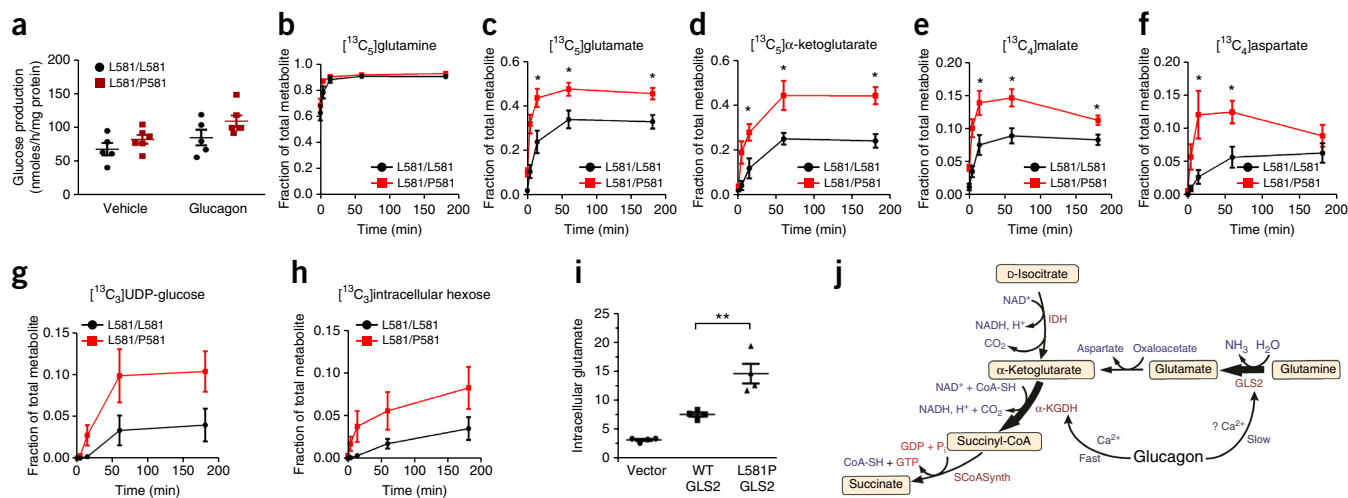


Figure 4 Glutamine metabolism in primary cryopreserved human hepatocytes from donors genotyped to be homozygous (L581/L581) and heterozygous (L581/P581) at *GLS2*. (a) Glucose production in the presence of glucagon or PBS vehicle for 1 h with extracellular glutamine, lactate, and pyruvate substrates. Values are from five (L581/L581) and six (L581/P581) donors, each representing the mean of three technical replicates. **P* < 0.05, two-way ANOVA. (b–h) Hepatocytes from donors with the L581/L581 and L581/P581 genotypes at *GLS2* were given [¹³C₅]glutamine and unlabeled lactate and pyruvate in kinetic flux studies. Intracellular [¹³C₅]glutamine (b), [¹³C₅]glutamate (c), [¹³C₅]α-ketoglutarate (d), [¹³C₄]malate (e), [¹³C₄]aspartate (f), [¹³C₃]UDP-glucose (g), and [¹³C₃]hexose (h) values were measured. Values represent the means of six biological replicates, each from a unique biological hepatocyte donor, for each group and time point, with each biological replicate representative of three technical replicates. Error bars, s.e.m. The steady-state data (from the 3-h time point) in this experiment were replicated in a separate study (data not shown). **P* < 0.05, two-tailed Student's *t*-test. (i) Intracellular glutamate levels were measured in immortalized human hepatocytes expressing either WT or L581P *GLS2*, with cells transduced with empty lentivirus vector as a control. Values represent the results from four biological replicates. ***P* < 0.01, two-tailed Student's *t*-test. (j) A model summarizing the proposed effects of glucagon on mitochondrial fluxes. IDH, isocitrate dehydrogenase; SCoASynth, succinate-CoA synthetase.

glucose production than control hepatocytes under basal conditions or after treatment with glucagon (Fig. 4a). Incubation of *GLS2* L581/P581 hepatocytes with [¹³C]glutamine and unlabeled lactate and pyruvate resulted in both more rapid labeling and greater enrichment at steady state than was observed for homozygous L581/L581 hepatocytes of multiple TCA and gluconeogenic intermediates (Fig. 4b–h). This increased labeling of TCA intermediates occurred despite equivalent fractional enrichment in intracellular glutamine, implicating a higher rate of glutamine-to-glutamate flux in the L581/P581 hepatocytes. To confirm that the *GLS2* mutation encoding p.Leu581Pro is a gain-of-function mutation, we overexpressed either WT or L581P *GLS2* in immortalized human hepatocytes and measured intracellular glutamate levels. Consistent with previous reports^{10,11}, exogenous expression of WT *GLS2* significantly increased intracellular glutamate, while expression of L581P *GLS2* further elevated intracellular glutamate levels (Fig. 4i). These data, in combination with the higher blood glucose levels in individuals with *GLS2* p.Leu581Pro variants, provide clear evidence that the contribution of glutaminolysis to gluconeogenesis is physiologically significant and of sufficient magnitude to impact glucose homeostasis in humans.

In addition to the absolute rate of gluconeogenesis, the supply of major gluconeogenic substrates is a critical factor necessary for sustained gluconeogenesis during fasting. Accelerated glutamine turnover has been observed in conditions associated with elevated glucagon levels *in vivo*, including fasting and exercise, physiological states that are also associated with a reduction in serum glutamine levels^{12–16}. Preferential utilization of glutamine under these conditions is likely related to the need for a stable pool of hepatic glucose precursors and the essential transfer of nitrogen from muscle amino acids to liver for conversion to urea and excretion^{12,17,18}. In this report, we have demonstrated a molecular mechanism by which glucagon biases

hepatic metabolism toward the utilization of glutamine. Unlike glucagon's effects on cytoplasmic enzyme activity, its mitochondrial actions serve to not only increase gluconeogenesis but also to modify substrate selection. While lactate accounted for the majority of the carbons destined for synthesis of glucose under both basal and hormone-stimulated conditions, glucagon stimulated a disproportionately greater increase in gluconeogenesis from glutamine. In this manner, glutaminolysis is responsible for the majority of the hormone-dependent increase in gluconeogenesis and probably contributes significantly to the rapid surge in mitochondrial respiration that has been long recognized as an important component of glucagon's actions^{19,20}. Thus, the glucagon-dependent shift to glutamine utilization is critical for the liver and organism during fasting states.

The kidney is also capable of glutamine-derived gluconeogenesis²¹. The fractional contribution of glutamine to renal gluconeogenesis is greater than that in the liver¹³. However, the impact of glucagon on glutamine-derived gluconeogenesis is restricted to the liver; increases in glucagon are capable of augmenting the hepatic glutamine-derived gluconeogenic rate to a level that surpasses the rate of glutamine-derived renal gluconeogenesis¹³. Therefore, glucagon signaling and systemic tone result not only in a change in hepatic gluconeogenic substrate selection but also in a change in the major sites of systemic consumption of this amino acid.

There have been previous indications that glucagon regulates mitochondrial metabolism. Glucagon elicits a rapid and significant enhancement of mitochondrial Ca²⁺ uptake, driven by glucagon-stimulated increases in cytoplasmic Ca²⁺ concentration due to release from intracellular stores^{22–25} and Ca²⁺ influx across the plasma membrane^{26,27}. The former has been proposed to be due to PKA-mediated phosphorylation of IP₃R (ref. 8). One consequence of activating IP₃R-mediated Ca²⁺ release is the efficient transfer of Ca²⁺ into

mitochondria, where it activates dehydrogenases and stimulates TCA cycle activity²⁸. In hepatocytes, glucagon reduces cellular α -ketoglutarate and activates AKGDH^{29,30}. In the current study, we have confirmed and extended these observations and can now integrate them into a coherent and quantitative model of how glucagon rapidly activates preferential flux from glutamine into glucose (Fig. 4j). Moreover, we have provided the first genetic evidence that this pathway is quantitatively significant in human liver. We propose that PKA-dependent phosphorylation of IP₃R leads to Ca²⁺ release from the ER, raising mitochondrial matrix Ca²⁺ concentrations with consequent AKGDH activation, stimulation of mitochondrial respiration and reduction of the levels of α -ketoglutarate. The ability of both glucagon and phenylephrine to promote the anaplerotic entry of substrate into the TCA cycle as α -ketoglutarate emphasizes the critical role of Ca²⁺ as a signaling intermediate. Glucagon also activates glutaminolysis, resulting in increased cellular glutamate content and ¹³C enrichment from glutamine in both mouse and human hepatocytes; however, the precise mechanisms for this remain unclear^{31,32}. Glucagon has also been shown to increase the rate of glutamine transport in conjunction with increased glutaminase activity³³; our work does not formally distinguish between these two points of flux control, but our data showing no increase in hepatocyte glutamine levels following glucagon treatment despite increased cellular glutamate would suggest that glutamine transport is a minor contributor.

The absence of GLS2 protein completely blocked the flux from glutamine to glucose in primary hepatocytes. Consistent with glutamine serving as a major glucagon-stimulated gluconeogenic substrate, GLS2-KO hepatocytes had minimal glucagon stimulation when a physiological mixture of lactate and glutamine was used as substrate. Glutamine flux appears to represent a quantitatively significant contributor to systemic glucose production in mice and humans, as indicated by the increase in plasma glucose elicited by a gain-of-function polymorphism in the *GLS2* gene in humans and the removal of GLS2 in mice. It is likely that the glucagon-dependent activation of hepatic glutaminolysis is an important component of both normal variation in circulating metabolites and the pathophysiology of type 2 diabetes. These studies raise the intriguing possibility that *GLS2* could represent a novel, genetically validated type 2 diabetes target for improvement of glucose homeostasis.

METHODS

Methods, including statements of data availability and any associated accession codes and references, are available in the [online version of the paper](#).

Note: Any Supplementary Information and Source Data files are available in the online version of the paper.

ACKNOWLEDGMENTS

All data generated and analyzed within this study are presented in the article and supplementary procedures. The stable-isotope-based metabolomics work was supported by US NIH grant CA211437 to W.L. This work was also supported by FONDECYT grant 1160332 to C.C. and CONICYT/FONDAP 15150012 to C.C.

AUTHOR CONTRIBUTIONS

R.A.M. designed and performed all experiments and drafted and edited the manuscript. Y.S. designed and performed experiments related to GLS2 knockout and *in vivo* infusion and drafted and edited the manuscript. W.L. performed mass spectrometry experiments in rodent cells and tissues and edited the manuscript. D.A.P. performed mass spectrometry experiments in human hepatocytes and edited the manuscript. A.J. performed experiments on human hepatocytes and edited the manuscript. M.B. performed mass spectrometry experiments in human

hepatocytes and edited the manuscript. H.W. performed experiments on human hepatocytes and edited the manuscript. C.C. performed mouse hepatocyte calcium experiments and edited the manuscript. M.W. performed experiments related to GLS2 knockout and *in vivo* infusions and edited the manuscript. J.K.F. edited the manuscript. J.O.P. performed flux modeling experiments and edited the manuscript. Y.Z. performed pancreas histology experiments and edited the manuscript. W.L.H. designed pancreas histology experiments and edited the manuscript. J.D.R. designed experiments and drafted and edited the manuscript. M.J.B. designed experiments and drafted and edited the manuscript.

COMPETING INTERESTS

R.A.M., Y.S., D.A.P., A.J., M.B., H.W., M.W., and M.J.B. were employed by Pfizer during the reported studies.

Reprints and permissions information is available online at <http://www.nature.com/reprints/index.html>. Publisher's note: Springer Nature remains neutral with regard to jurisdictional claims in published maps and institutional affiliations.

1. Miller, R.A. & Birnbaum, M.J. Glucagon: acute actions on hepatic metabolism. *Diabetologia* **59**, 1376–1381 (2016).
2. Scott, R.A. *et al.* Large-scale association analyses identify new loci influencing glycemic traits and provide insight into the underlying biological pathways. *Nat. Genet.* **44**, 991–1005 (2012).
3. Suhre, K. *et al.* Human metabolic individuality in biomedical and pharmaceutical research. *Nature* **477**, 54–60 (2011).
4. Exton, J.H. & Park, C.R. Control of gluconeogenesis in liver. II. Effects of glucagon, catecholamines, and adenosine 3',5'-monophosphate on gluconeogenesis in the perfused rat liver. *J. Biol. Chem.* **243**, 4189–4196 (1968).
5. Young, V.R. & Ajami, A.M. Glutamine: the emperor or his clothes? *J. Nutr.* **131**, 2449S–2459S discussion 2486S–2447S (2001).
6. Miller, R.A. *et al.* Biguanides suppress hepatic glucagon signalling by decreasing production of cyclic AMP. *Nature* **494**, 256–260 (2013).
7. Titchenell, P.M. *et al.* Direct hepatocyte insulin signaling is required for lipogenesis but is dispensable for the suppression of glucose production. *Cell Metab.* **23**, 1154–1166 (2016).
8. Williamson, J.R. *et al.* Mechanisms involved in receptor-mediated changes of intracellular Ca²⁺ in liver. *Soc. Gen. Physiol. Ser.* **42**, 93–116 (1987).
9. Watford, M. & Smith, E.M. Distribution of hepatic glutaminase activity and mRNA in perivenous and periportal rat hepatocytes. *Biochem. J.* **267**, 265–267 (1990).
10. Hu, W. *et al.* Glutaminase 2, a novel p53 target gene regulating energy metabolism and antioxidant function. *Proc. Natl. Acad. Sci. USA* **107**, 7455–7460 (2010).
11. Suzuki, S. *et al.* Phosphate-activated glutaminase (GLS2), a p53-inducible regulator of glutamine metabolism and reactive oxygen species. *Proc. Natl. Acad. Sci. USA* **107**, 7461–7466 (2010).
12. Krishna, M.G. *et al.* Glucagon response to exercise is critical for accelerated hepatic glutamine metabolism and nitrogen disposal. *Am. J. Physiol. Endocrinol. Metab.* **279**, E638–E645 (2000).
13. Stumvoll, M., Meyer, C., Kreider, M., Perriello, G. & Gerich, J. Effects of glucagon on renal and hepatic glutamine gluconeogenesis in normal postabsorptive humans. *Metabolism* **47**, 1227–1232 (1998).
14. Battezzati, A., Simonson, D.C., Luzi, L. & Matthews, D.E. Glucagon increases glutamine uptake without affecting glutamine release in humans. *Metabolism* **47**, 713–723 (1998).
15. Hankard, R.G., Haymond, M.W. & Darmaun, D. Role of glutamine as a glucose precursor in fasting humans. *Diabetes* **46**, 1535–1541 (1997).
16. Stumvoll, M. *et al.* Glutamine and alanine metabolism in NIDDM. *Diabetes* **45**, 863–868 (1996).
17. Perriello, G. *et al.* Estimation of glucose–alanine–lactate–glutamine cycles in postabsorptive humans: role of skeletal muscle. *Am. J. Physiol.* **269**, E443–E450 (1995).
18. Nurjhan, N. *et al.* Glutamine: a major gluconeogenic precursor and vehicle for interorgan carbon transport in man. *J. Clin. Invest.* **95**, 272–277 (1995).
19. Halestrap, A.P. Stimulation of the respiratory chain of rat liver mitochondria between cytochrome c₁ and cytochrome c by glucagon treatment of rats. *Biochem. J.* **172**, 399–405 (1978).
20. Yamazaki, R.K. Glucagon stimulation of mitochondrial respiration. *J. Biol. Chem.* **250**, 7924–7930 (1975).
21. Stumvoll, M., Perriello, G., Meyer, C. & Gerich, J. Role of glutamine in human carbohydrate metabolism in kidney and other tissues. *Kidney Int.* **55**, 778–792 (1999).
22. Mauger, J.P., Claret, M., Pietri, F. & Hilly, M. Hormonal regulation of inositol 1,4,5-trisphosphate receptor in rat liver. *J. Biol. Chem.* **264**, 8821–8826 (1989).
23. Burgess, G.M., Bird, G.S., Obie, J.F. & Putney, J.W. Jr. The mechanism for synergism between phospholipase C- and adenylcyclase-linked hormones in liver. Cyclic AMP-dependent kinase augments inositol trisphosphate-mediated Ca²⁺ mobilization without increasing the cellular levels of inositol polyphosphates. *J. Biol. Chem.* **266**, 4772–4781 (1991).

24. Bygrave, F.L., Gamberucci, A., Fulceri, R. & Benedetti, A. Evidence that stimulation of plasma-membrane Ca^{2+} inflow is an early action of glucagon and dibutyryl cyclic AMP in rat hepatocytes. *Biochem. J.* **292**, 19–22 (1993).
25. Fernando, K.C., Gregory, R.B. & Barritt, G.J. Protein kinase A regulates the disposition of Ca^{2+} which enters the cytoplasmic space through store-activated Ca^{2+} channels in rat hepatocytes by diverting inflowing Ca^{2+} to mitochondria. *Biochem. J.* **330**, 1179–1187 (1998).
26. Hughes, B.P. & Barritt, G.J. Effects of glucagon and N^6O^2' -dibutyryl adenosine 3':5'-cyclic monophosphate on calcium transport in isolated rat liver mitochondria. *Biochem. J.* **176**, 295–304 (1978).
27. Keppens, S., Vandenheede, J.R. & De Wulf, H. On the role of calcium as second messenger in liver for the hormonally induced activation of glycogen phosphorylase. *Biochim. Biophys. Acta* **496**, 448–457 (1977).
28. Denton, R.M. & McCormack, J.G. Ca^{2+} transport by mammalian mitochondria and its role in hormone action. *Am. J. Physiol.* **249**, E543–E554 (1985).
29. Siess, E.A. & Wieland, O.H. Glucagon-induced stimulation of 2-oxoglutarate metabolism in mitochondria from rat liver. *FEBS Lett.* **93**, 301–306 (1978).
30. Williamson, J.R., Browning, E.T., Thurman, R.G. & Scholz, R. Inhibition of glucagon effects in perfused rat liver by (+)decanoylcarnitine. *J. Biol. Chem.* **244**, 5055–5064 (1969).
31. Lacey, J.H., Bradford, N.M., Joseph, S.K. & McGivan, J.D. Increased activity of phosphate-dependent glutaminase in liver mitochondria as a result of glucagon treatment of rats. *Biochem. J.* **194**, 29–33 (1981).
32. Joseph, S.K. & McGivan, J.D. The effect of ammonium chloride and glucagon on the metabolism of glutamine in isolated liver cells from starved rats. *Biochim. Biophys. Acta* **543**, 16–28 (1978).
33. Low, S.Y., Salter, M., Knowles, R.G., Pogson, C.I. & Rennie, M.J. A quantitative analysis of the control of glutamine catabolism in rat liver cells. Use of selective inhibitors. *Biochem. J.* **295** (Pt. 2), 617–624 (1993).

ONLINE METHODS

Materials. AAV-PKA-DN virus was constructed by cloning a cDNA encoding dominant inhibitory PKA-Rlab into an AAV plasmid that contained a hepatocyte-specific promoter (thyroid-binding globulin, *Tbg*)³³. An shRNA targeting the mouse *Gls2* gene was created that had the 21-nucleotide sequence 5'-GCGTATTTGAGGATGCCAAAG-3' after the U6 promoter in an AAV vector. AAV virus was produced at the University of Pennsylvania Vector Core. Stable-isotope substrates were purchased from Cambridge Isotopes. All other chemicals were purchased from Sigma-Aldrich. Antibodies specific for phosphorylated (Ser1756; 8548) and total (8568) IP₃R, phosphorylated (Ser133; 9198) and total (9197) CREB, phosphorylated (Tyr1150/1151; 3204) and total (3205) insulin receptor β , phosphorylated (Ser473; 4060) and total (4691) Akt, total GAPDH (5174) and β -actin (3700) were purchased from Cell Signaling Technology. Total PFKFB1 antibody was purchased from Abcam (ab71625). Total GLS2 antibody was purchased from Sigma (HPA038608). The antibody to phosphorylated (Ser33) PFKFB1 was produced by Cell Signaling Technology⁶. Cryopreserved human hepatocytes were purchased from BD Biosciences. Immortalized human hepatocytes were purchased from ATCC. Lentivirus for GLS2 overexpression was constructed by cloning cDNA expressing either WT or L581P GLS2 into the pCDH expression lenti-vector from System Biosciences. The Amplex Red Glutamic Acid/Glutamate Oxidase Assay kit was purchased from Thermo Fisher Scientific. An ultra-sensitive mouse insulin ELISA kit was obtained from Crystal Chem. The Glucagon 10 μ l ELISA kit was purchased from Mercodia. The Glutamine Assay kit (KA1627) was from Abnova.

***Gls2*-knockout mice.** Mice with constitutive knockout of the *Gls2* gene via Cas9-mediated gene editing were created and provided by Taconic Biosciences. The targeting strategy involved co-injection of the *Cas9* mRNA together with the proximal and distal sgRNAs into C57BL/6NTac zygotes, resulting in deletion of exons 2–7 of the *Gls2* gene. The analysis of off-target effects was based on the GRCm38/mm10 assembly. The analysis of potential non-intergenic off-target sites was performed in the G₁ generation, and none of the off-target sites were found.

***In vivo* and primary hepatocyte glucose output studies.** All animal studies followed ethical guidelines and were approved by the University of Pennsylvania or Pfizer IACUC. *In vivo* animal studies were performed in 12-week-old male C57BL/6 mice and were not performed with randomization or blinding. Primary hepatocytes were isolated from male C57BL/6 mice from 12–18 weeks of age by the two-step collagenase perfusion method using Liver Digest reagents from Invitrogen³⁴. After isolation, cells were plated in M199 medium with 10% FBS for 3 h in multiwell plates precoated with collagen I. After cells attached to the plates, they were washed with glucose output medium (GOM) (118 mM NaCl, 4.7 mM KCl, 1.2 mM MgSO₄, 1.2 mM KH₂PO₄, 1.2 mM CaCl₂, 20 mM NaCO₃, 25 mM HEPES pH 7.4, and 0.025% BSA) and incubated in fresh GOM for 1 h. GOM was replaced with fresh, prewarmed GOM, and cellular treatments were initiated. For glucose output studies, the cells were given the indicated gluconeogenic substrates and extracellular glucose was assayed after 1 h using a hexokinase-based glucose assay kit (Sigma-Aldrich); data were normalized to total cellular protein. Glucose production assays to quantify rates of lactate and glutamine consumption and pyruvate production for modeling purposes were performed by treating cells as above in glucose production assays with 5 mM [¹²C₃]lactate and 2.5 mM [¹²C₅]glutamine. At 30 min and 1 h, medium was removed, centrifuged to remove loose cells, and an equal volume of methanol containing 5 mM [¹³C₃]lactate, 2.5 mM [¹³C₅]glutamine, 0.5 mM [¹³C₁]pyruvate, and 0.5 mM [¹³C₆]glucose was added. After removal of medium, cells were lysed and protein was measured. Medium–methanol mixtures were analyzed by mass spectrometry, and rates of metabolite production and consumption were measured.

Glutamine infusion studies. Twelve-week-old C57BL/6 mice were purchased from Jackson Laboratories with an indwelling jugular vein catheter. Four days after arrival, animals were infected with AAV-GFP or AAV-GLS2-sh at a dose of 10¹¹ viral genomes per animal. Two weeks after infection, mice were fasted

beginning at 6 a.m., and lines were flushed with heparin in saline and hooked up to infusion pumps. After 4 h of fasting, pumps began to infuse animals with 0.25 mmol/kg/h [U-¹³C]glutamine for 1 h. After 1 h, the pump solutions were switched to include either 0.25 mmol/kg/h [U-¹³C]glutamine or 0.25 mmol/kg/h [U-¹³C]glutamine with the addition of 1 mg/kg/h of glucagon. After 1 h of infusion, animals were anesthetized with pentobarbital, liver tissue was collected and rapidly frozen in liquid nitrogen, and terminal blood was collected by cardiac stick.

Mass spectrometry. Primary hepatocytes were given the indicated gluconeogenic substrates, and reactions were stopped by rapidly removing culture medium and adding to the cells 80% methanol precooled with dry ice. Cellular debris was removed by centrifugation, and samples were dried by speedvac. The dried cell extracts were redissolved in 200 μ l of HPLC-grade water and analyzed via reverse-phase ion-pairing chromatography coupled to an Exactive orbitrap mass spectrometer (Thermo Fisher Scientific). The mass spectrometer was operated in negative-ion mode with a scan rate of 1 Hz and a resolving power of 100,000, with a scanning range of *m/z* 85–1,000. The LC method has been described before³³, using a Synergy Hydro-RP column (100 mm \times 2 mm, particle size of 2.5 μ m, Phenomenex) with a flow rate of 200 μ l/min. The LC gradient was as follows: 0 min, 0% B; 2.5 min, 0% B; 5 min, 20% B; 7.5 min, 20% B; 13 min, 55% B; 15.5 min, 95% B; 18.5 min, 95% B; 19 min, 0% B; 25 min, 0% B. Solvent A was 97:3 water:methanol with 10 mM tributylamine and 15 mM acetic acid; solvent B was methanol. Other LC parameters were as follows: autosampler temperature, 5 $^{\circ}$ C; injection volume, 10 μ l; column temperature, 25 $^{\circ}$ C.

Data analyses were performed using MAVEN software⁶, which performs both peak alignment and quantification (for both labeled and unlabeled forms) and allows user validation by extracted ion chromatogram visualization. All peak identities were confirmed by exact mass and retention time matching to authenticated metabolite standards. Ion signals were further processed to correct for the natural isotope abundance of the unlabeled glucose and trace unlabeled impurity in the labeled substrates.

Metabolic flux analysis. Mass isotopomer distributions of intracellular and extracellular metabolites were obtained via LC–MS when cells were incubated with [¹³C₅]glutamine or [¹³C₃]lactate. Intracellular metabolites, glucose-6-phosphate, glycerol-3-phosphate (a proxy for dihydroxyacetone phosphate), 3-phosphoglycerate, phosphoenolpyruvate, pyruvate, acetyl-CoA, α -ketoglutarate, succinate, malate, aspartate (a proxy for cytosolic oxaloacetate), and glutamate were included in the flux calculation. In addition, measured lactate and glutamine uptake rates as well as glucose and pyruvate secretion rates were input. The lactate exchange rate, that is, the rate at which [¹³C]lactate appeared in the medium when [¹³C]glutamine and [¹²C]lactate were used as carbon sources, was measured. A cumomer network encompassing TCA cycle, anaplerotic, and gluconeogenic reactions was generated using 13CFLUX2 (<http://www.13cflux.net/>)^{4,34}. The flux distributions that minimized the variance-weighted sum of the squared residuals between measured and computed mass isotopomer distributions were obtained by iteratively invoking the interior-point optimization algorithm in Matlab. Subsequently, 95% confidence intervals around the optimal fluxes were calculated³⁵.

α -Ketoglutarate assays. Primary hepatocytes were incubated with 5 mM lactate for 30 min and then treated as indicated. Reactions were stopped by removing the culture medium, and α -ketoglutarate was extracted with the addition of 80% methanol. Cellular debris was removed by centrifugation, and samples were dried by speedvac. α -Ketoglutarate and pyruvate were quantified in coupled glutamic transaminase and pyruvate oxidase reactions in the presence of horseradish peroxidase and Amplex Red³⁶. Briefly, reactions containing 100 mM KPO₄ pH 6.8, 1 mM EDTA, 1 mM MgCl₂, 10 μ M FAD, 200 μ M TPP, 20 mM alanine, 25 μ M Amplex Red, 0.5 U/ml horseradish peroxidase, 0.2 U/ml pyruvate oxidase, and \pm 0.2 units/ml glutamic pyruvic transaminase were incubated for 30 min with samples or α -ketoglutarate standards. Amplex Red fluorescence was quantified with excitation by 535-nm light, detecting emission at 587 nm, and values from samples lacking transaminase were subtracted from those for transaminase-containing samples.

α -Ketoglutarate dehydrogenase assays. For AKGDH assays, mitochondria were isolated by differential centrifugation from primary hepatocytes treated as indicated³⁷. The assay buffer included 20 mM HEPES pH 7.4, 1 mM MgCl₂, 100 μ M CoA, 2.5 mM NAD⁺, 0.01% rotenone, 2 mM KCN, and 1 mM DTT \pm 50 μ M α -ketoglutarate. Assays were started by addition of mitochondria, and NADH production was monitored by the absorbance at 340 nm.

Calcium measurements. Freshly isolated primary hepatocytes from WT C57BL/6 mice were plated on collagen-coated coverslips, allowed to attach for 3 h, and loaded with Fura-2 dye. Images were acquired with a continuous flow of medium for rapid switching of treatment conditions. Fluorescence ratios were compared to standard curves to estimate total cytoplasmic calcium levels.

Human hepatocyte genotyping. Forty-one cryopreserved human hepatocyte lots were purchased from BD Biosciences and Life Technologies. Genomic DNA was extracted using the QIAamp DNA Micro kit (Qiagen) in accordance with the manufacturer's instructions. DNA was resuspended to a concentration of 5–10 ng/ μ l for subsequent genotyping analysis. Genotyping of rs2657879 (c.1742T>C) was performed following amplification of the 411-bp genomic sequence using the primers rs2657879F (5'-TTTGCCAAGGACAGGTGAGG-3') and rs2657879R (5'-CTTGGTCCCCACTGAAGCAG-3'). The PCR product was sent to Beckman Coulter Genomics for direct sequencing using the primer rs2657879seq (5'-TTTGCCAAGGACAGGTGAGG-3').

Cryopreserved human hepatocyte culture. Cryopreserved human hepatocytes were thawed in High-Viability CryoHepatocyte Recovery Medium (454560, BD Biosciences). Nonviable cells were removed following the cell vendor's protocol before cell plating. Viable cells were plated onto collagen-coated 48-well plates (150,000 cells/well) in Invitrogen plating medium (Celsis IVT Z99029, Bioreclemation IVT) and were allowed to attach for 6 h. After attachment, the medium was replaced with fresh low-glucose DMEM supplemented with 10% FBS and 1 μ M glucagon (G3157, Sigma-Aldrich). The following day, cells were incubated in Krebs buffer for 1 h without gluconeogenic substrates. At time 0, the medium was switched to medium with 5 mM [¹²C₃]lactate, 0.5 mM [¹²C₃]pyruvate, and 2.5 mM [¹³C₅]glutamine. Cells were incubated for 1, 5, 15, 60, or 180 min, washed in warm PBS, and lysed with the addition of cold 80% methanol. Cells were scraped, and cellular debris was pelleted through centrifugation. Supernatants were collected, dried under vacuum, and reconstituted in 100 μ l of 0.1% formic acid before LC-HRMS analysis.

Immunofluorescence of pancreatic islets. Immunofluorescent staining for insulin and glucagon was performed as previously described on multiple, non-adjacent 5- μ m sections no closer than 50 μ m apart³⁸. Antibody to glucagon was from Abcam (10988; 1:1,000 dilution), and antibody to insulin was from Dako (A0564; 1:500 dilution). Images were collected using a BZ-X710 fluorescence microscope (Keyence).

LC-HRMS analysis and workflow. Analysis of glutamine and its cellular metabolites was conducted by injecting a 10- μ l sample aliquot onto an Imtakt UK-Phenyl (2.1 mm \times 150 mm) column (Imtakt USA) using a Waters Acquity UPLC system (Waters Corp.) coupled to a Thermo Q-Exactive (Thermo Corp.) mass spectrometer. Analytes were chromatographically resolved using a

linear gradient from 0% to 50% B or acetonitrile containing 0.3% formic acid, over 3 min at 500 μ l/min with a column temperature of 40 °C. Mobile phase A composition was 0.1% formic acid. Metabolites were monitored using negative-ion electrospray (ESI⁻) in full scan mode with a resolution of 70,000 calibrated to mass accuracy <2 p.p.m. Instrument parameters were fixed: the sheath gas was 60 instrument-specific arbitrary units (AU), the auxiliary gas was 40 AU, the sweep gas was 2 AU, the ESI⁻ spray voltage was -3 kV, the capillary temperature was 320 °C, and the S-lens was set at 50 AU. Glutamine flux was determined through measurement of expected ¹³C glutaminolysis isotopomers. Cell experiments without the addition of labeled glutamine were used as negative controls to ensure that the labeled metabolites identified were unique to the samples treated with labeled substrate. Thermo LCQuan (Thermo Corp.) was used to extract out exact mass, extracted ion chromatograms using a window of 10 p.p.m. at the calculated accurate mass for each metabolite and isotopomer. Individual isotopomer percentages were normalized to the total sum of all detected isotopomers after natural isotope correction. Data analysis was performed using Microsoft Excel, and plots were generated in GraphPad Prism.

Statistics. All results are expressed as means \pm s.e.m. All two-group comparisons were deemed statistically significant by unpaired two-tailed Student's *t*-test if *P* < 0.05 or by two-way ANOVA. All experimental values were obtained from the measurement of distinct samples and non-repeated measures of the same sample. Experiments were performed multiple times as indicated in the figure legends, with representative data presented. Sample sizes were selected on the basis of previous knowledge of the variation in experimental methods and the expected effect size observed in previous studies. Variation was similar between groups being compared and exhibited apparent normal distribution.





General methods statements. No samples, mice, or studies were removed from the analyses. Experiments were not blinded and samples were not randomized in this study, except for the analysis of mass spectrometry samples, which were run agnostic of groupings. Tissue culture samples were not evaluated for mycoplasma contamination.

Life Sciences Reporting Summary. Further information on experimental design is available in the **Life Sciences Reporting Summary**.

Data availability. All analyses are contained within this manuscript, and source data are archived and available upon reasonable request. Uncropped images of western blots can be found in **Supplementary Figure 7**.

34. Lu, W. *et al.* Metabolomic analysis via reversed-phase ion-pairing liquid chromatography coupled to a stand alone orbitrap mass spectrometer. *Anal. Chem.* **82**, 3212–3221 (2010).
35. Melamud, E., Vastag, L. & Rabinowitz, J.D. Metabolomic analysis and visualization engine for LC-MS data. *Anal. Chem.* **82**, 9818–9826 (2010).
36. Weitzel, M. *et al.* 13CFLUX2—high-performance software suite for ¹³C-metabolic flux analysis. *Bioinformatics* **29**, 143–145 (2013).
37. Wiechert, W., Mollney, M., Isermann, N., Wurzel, M. & de Graaf, A.A. Bidirectional reaction steps in metabolic networks: III. Explicit solution and analysis of isotopomer labeling systems. *Biotechnol. Bioeng.* **66**, 69–85 (1999).
38. Antoniewicz, M.R., Kelleher, J.K. & Stephanopoulos, G. Determination of confidence intervals of metabolic fluxes estimated from stable isotope measurements. *Metab. Eng.* **8**, 324–337 (2006).

Publisher Correction: Targeting hepatic glutaminase activity to ameliorate hyperglycemia

Russell A. Miller, Yuji Shi, Wenyun Lu, David A. Pirman, Aditi Jatkar, Matthew Blatnik, Hong Wu, César Cárdenas, Min Wan, J. Kevin Foskett , Junyoung O. Park , Yiyi Zhang, William L. Holland , Joshua D. Rabinowitz and Morris J. Birnbaum 

Correction to: *Nature Medicine* <https://doi.org/10.1038/nm.4514>, published online 26 March 2018.

In the version of this article initially published, the “[¹³C₂]α-ketoglutarate” label on Fig. 1g is incorrect. It should be “[¹³C₅]α-ketoglutarate”. Additionally, in Fig. 3b, the “AAV-GFP” group is missing a notation for significance, and in Fig. 3c, the “AAV-GLS2-sh” group is missing a notation for significance. There should be a double asterisk notating significance in both panels. Finally, in the Fig. 4g legend, “[¹³C₆]UDP-glucose” should be “[¹³C₃]UDP-glucose”, and in the Fig. 4h legend, “[¹³C₆]hexose” should be “[¹³C₃]hexose”. The errors have been corrected in the HTML and PDF versions of this article.

Published online: 12 June 2018

<https://doi.org/10.1038/s41591-018-0047-1>